Available online at www.sciencedirect.com
SCIENCE DIRECT®
Journal of Magnetic Resonance 177 (2005) 31–43
JMR Journal of Magnetic Resonance
www.elsevier.com/locate/jmr

Active shielding of cylindrical saddle-shaped coils: Application to wire-wound RF coils for very low field NMR and MRI

C.P. Bidinosti *, I.S. Kravchuk, M.E. Hayden

Department of Physics, Simon Fraser University, Burnaby, BC, Canada V5A 1S6

Received 23 March 2005; revised 30 June 2005
Available online 11 August 2005

Abstract

We provide an exact expression for the magnetic field produced by cylindrical saddle-shaped coils and their ideal shield currents in the low-frequency limit. The stream function associated with the shield surface current is also determined. The results of the analysis are useful for the design of actively shielded *radio-frequency* (RF) coils. Examples pertinent to very low field nuclear magnetic resonance (NMR) and magnetic resonance imaging (MRI) are presented and discussed.

PACS: 07.55.Db; 84.32.Hh; 41.20.Gz; 87.61.Ff

Keywords: Saddle-shaped coils; Transmit and receive coils; Active shielding; Low frequency magnetic fields; Low field magnetic resonance

1. Introduction

A saddle-shaped coil produces a central magnetic field that is transverse to its cylindrical axis, and thus constitutes an appropriate building-block for the construction of wire-wound transmit and/or receive coils to be used within solenoidal MR magnets. While the low self-resonance frequency of wire-wound RF coils—due to stray capacitance [1]—tends to preclude their use in most NMR and MRI applications, a growing interest in very low field techniques (e.g., prepolarization [2,3], hyperpolarized gases [4–6]) provides strong motivation to explore the design of such coils in much greater detail. This is underscored by the fact that typical RF resonator designs—such as the birdcage resonator [1,7,8]—are poorly suited for low-frequency operation, owing to the increased difficulty of tuning their inherently low self-inductance [9]. We use the cylindrical saddle-shaped current element shown in Fig. 1 as the elementary building-block from which shielded RF coils, suitable for low-frequency operation, can be constructed.

The task of shielding the magnetic field produced by low-frequency coils is nontrivial and generally requires the use of active rather than passive shields [10,11]. This approach has been applied widely to the design of gradient coils [12,7] as well as to shim coils [13]. Passive shielding of RF coils is more convenient in high-frequency applications where a simple metallic enclosure of sufficient thickness will support the induced surface current (i.e., eddy current) flow needed to contain B_1 fields or screen spurious external fields. This approach becomes problematic if the RF frequency is comparable to or less than the switching frequency of applied gradient fields, since a shield designed to contain the former will also exclude the latter. In this case, one must resort to active shielding. Here the metallic enclosure is replaced by a distribution of wires that, when driven by an appropriate current, simulates the surface current that would otherwise have been induced on the enclosure by the RF field. The design of the active shield is

* Corresponding author. Fax +1 604 291 3592.
E-mail address: cpbidino@sfu.ca (C.P. Bidinosti).

1090-7807/$ - see front matter © 2005 Elsevier Inc. All rights reserved.
doi:10.1016/j.jmr.2005.07.003

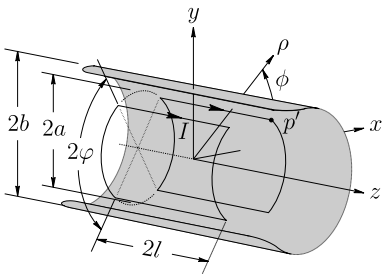

Fig. 1. The geometry of the cylindrical saddle-shaped coil. The vertex p' is the point (a, φ, l) in cylindrical coordinates. The current I produces a transverse magnetic field along the x-direction at the coil isocenter. The appropriate current distribution on the surface $\rho = b$ (cut away) will completely cancel the field beyond this radius.

determined from a knowledge of this shield surface current, which in turn is linked to the current configuration of the RF coil via its magnetic field [11].

The magnetic field of the unshielded saddle-shaped coil has been studied previously by many authors [14–22]. For example, Ginsberg and Melchner [15] give the field at the isocenter of the coil and determine conditions for minimizing its second derivatives; Hoult [17] provides an expansion about the isocenter in terms of an infinite series of spherical harmonics; while Hanssum [19] calculates an exact solution in terms of elliptic integrals. In this work, we follow the approach of Turner and Bowley [11] and write the magnetic field of the perfectly shielded saddle-shaped coil using a Green function[1] expansion. The analysis gives an exact solution for the shield surface current in terms of the coil parameters and can be used to design actively driven shields.

1.1. Outline

This paper is arranged as follows. In Section 2, a general formula for the magnetic field of cylindrically constrained surface currents is provided, and the condition for perfect shielding is determined. We discuss the concept of the stream function [24] and derive a means for determining discrete current approximations to the surface currents of interest here. In Section 3, we use these general results to derive the corresponding expressions for the cylindrical saddle-shaped coil. We analyze the transverse magnetic field component of the perfectly shielded coil and discuss optimization of its homogeneity. In Section 4, two examples are presented that demonstrate the utility of this work for the design of actively shielded RF coils suitable for low-frequency NMR and MRI. Finally, a number of appendices are provided to give details of derivations, show correspondence to well known results, and collect important conceptual knowledge about transverse magnetic field generation.

2. Cylindrically constrained surface currents

2.1. The magnetic field

In cylindrical coordinates, a current density constrained to the surface $\rho = s$ is written

$$\boldsymbol{J} = \left[F_\phi(\phi, z)\boldsymbol{e}_\phi + F_z(\phi, z)\boldsymbol{e}_z\right]\delta(\rho - s), \tag{1}$$

where $F_\phi(F_z)$ is the surface current component in the azimuthal (axial) direction and $\delta(\zeta)$ is the Dirac delta function. The magnetic field produced by $\boldsymbol{J}$ can be expressed in terms of a Fourier expansion of F_ϕ and F_z [11]. The Fourier components are given by

$$\left.\begin{matrix} F_\phi^m(k) \\ F_z^m(k) \end{matrix}\right\} = \frac{1}{2\pi}\int_{-\pi}^{\pi} \mathrm{d}\phi\, \mathrm{e}^{-\mathrm{i}m\phi} \int_{-\infty}^{\infty} \mathrm{d}z\, \mathrm{e}^{-\mathrm{i}kz} \left\{\begin{matrix} F_\phi(\phi, z) \\ F_z(\phi, z) \end{matrix}\right. \tag{2}$$

and are linked to one another through the relationship

$$mF_\phi^m(k) = -ksF_z^m(k), \tag{3}$$

which follows from the equation of continuity, $\nabla \cdot \boldsymbol{J} = 0$ [11]. Using Eq. (3), a very compact form of the magnetic field can be written in terms of either the azimuthal or axial Fourier components of the surface current (see Appendix A for details).

For the specific case of interest in this paper, where we consider currents $\boldsymbol{J} = \boldsymbol{F}\,\delta(\rho - a)$ and $\boldsymbol{j} = \boldsymbol{f}\,\delta(\rho - b)$, the components of the magnetic field are

$$\begin{pmatrix} B_\rho \\ B_\phi \\ B_z \end{pmatrix} = \frac{\mu_o}{2\pi}\sum_{m=-\infty}^{\infty} \mathrm{e}^{\mathrm{i}m\phi} \int_{-\infty}^{\infty} \mathrm{d}k\, \mathrm{e}^{\mathrm{i}kz} \times \begin{pmatrix} \frac{k^2}{\mathrm{i}m}\left[a^2 P_m(a) F_z^m(k) + b^2 P_m(b) f_z^m(k)\right] \\ \frac{k}{\rho}\left[a^2 Q_m(a) F_z^m(k) + b^2 Q_m(b) f_z^m(k)\right] \\ \frac{k^2}{m}\left[a^2 Q_m(a) F_z^m(k) + b^2 Q_m(b) f_z^m(k)\right] \end{pmatrix}, \tag{4}$$

where we define the functions

$$P_m(s) = \begin{cases} I_m'(k\rho)K_m'(ks), & \text{when } \rho < s \\ I_m'(ks)K_m'(k\rho), & \text{when } \rho > s \end{cases} \tag{5}$$

and

$$Q_m(s) = \begin{cases} I_m(k\rho)K_m'(ks), & \text{when } \rho < s \\ I_m'(ks)K_m(k\rho), & \text{when } \rho > s \end{cases} \tag{6}$$

with $I_m(K_m)$ being the modified Bessel function of the first (second) kind and $I_m'(K_m')$ its derivative. The magnetic field may be equivalently written in terms of $F_\phi^m(k)$ and $f_\phi^m(k)$.[2] In either form, Eq. (4) is perfectly

[1] We adopt the nomenclature of Jackson (see Preface to the Second Edition [23]) and use the term "Green function" rather than "Green's function."

[2] As a matter of bookkeeping, the latter form is likely to be preferred in cases where the $m = 0$ component of an azimuthal current is nonzero.

general, describing completely the magnetic field that arises from any continuous surface currents $\boldsymbol{F}$ and $\boldsymbol{f}$ constrained to cylindrical surfaces $\rho = a$ and b, respectively. We also note that when it is written in this form, Eq. (4) is readily generalized to include contributions from currents on any number of coaxial cylindrical surfaces.

2.2. Perfect shielding

Inspection of Eq. (4) reveals that the condition for perfect shielding (i.e., $\boldsymbol{B} = 0$ for $\rho > b$) is satisfied when

$$f_z^m(k) = -\frac{a^2 I'_m(ka)}{b^2 I'_m(kb)} F_z^m(k), \tag{7}$$

or equivalently when

$$f_\phi^m(k) = -\frac{a I'_m(ka)}{b I'_m(kb)} F_\phi^m(k). \tag{8}$$

Eqs. (7) and (8) were originally derived by Turner and Bowley [11]. They allow one to determine the surface current $\boldsymbol{f}(\phi, z)$ on $\rho = b$ required to shield the magnetic field due to any continuous surface current $\boldsymbol{F}(\phi,z)$ from a known coil configuration on $\rho = a$.[3]

The inverse Fourier transform

$$\left.\begin{matrix} f_\phi(\phi,z) \\ f_z(\phi,z) \end{matrix}\right\} = \frac{1}{2\pi} \sum_{m=-\infty}^{\infty} \mathrm{e}^{\mathrm{i}m\phi} \int_{-\infty}^{\infty} \mathrm{d}k\, \mathrm{e}^{\mathrm{i}kz} \left\{\begin{matrix} f_\phi^m(k) \\ f_z^m(k) \end{matrix}\right. \tag{9}$$

gives the spatial components of the shield surface current. The objective for constructing actively driven shields is to approximate f_ϕ and f_z with discrete line currents. The use of the stream function, discussed below, facilitates this task.

2.3. The stream function

It follows from the general properties of a divergenceless vector field [25] that there exists a vector potential $\boldsymbol{\psi}$ such that:

$$\boldsymbol{j} = \nabla \times \boldsymbol{\psi} \tag{10}$$

for any continuous current density $\boldsymbol{j}$. For the class of problems considered here, where the current density $\boldsymbol{j} = \boldsymbol{f}(\phi, z)\delta(\rho - b)$ is constrained to a cylindrical surface, the vector potential need only have a single radial component $\boldsymbol{\psi} = \psi(\phi, z)\boldsymbol{e}_\rho$. The stream function ψ is related to the components of the surface current through the equations

$$f_\phi = \frac{\partial \psi}{\partial z} \text{ and } f_z = \frac{-1}{b}\frac{\partial \psi}{\partial \phi} \tag{11}$$

and can be determined from either once f_ϕ or f_z is known [24]. The stream function has the extremely useful properties that its contours are tangential to the flow lines of $\boldsymbol{f}$ on $\rho = b$ and that equispaced contours bound regions of equal integrated surface current. As a result, equispaced contours of ψ represent paths of equivalent line current and the stream function can be used to directly determine coil winding patterns that approximate the desired surface current [24].

The shield surface currents $\boldsymbol{f} = f_\phi(\phi,z)\boldsymbol{e}_\phi + f_z(\phi,z)\boldsymbol{e}_z$ to be considered in this work will have the same symmetry as the saddle-shaped coil: f_ϕ is cosine-symmetric in ϕ and an odd function of z, while f_z is sine-symmetric in ϕ and an even function of z. As a result, we can restrict our determination of wire positions to the first quadrant, i.e., $\phi = 0$ to $\pi/2$. To begin, we calculate the total current per quadrant flowing on a shield

$$I_s \equiv \int_0^{\pi/2} f_z(\phi, 0) b\, \mathrm{d}\phi, = \psi(0,0) \tag{12}$$

noting that $\psi(\pi/2, z) = 0$ due to symmetry. Now, if we are to approximate $\boldsymbol{f}$ using N wires per quadrant, each carrying the same in-phase current I_s / N, then the wires must be located along contours of the stream function displaced from one another by the amount $\psi(0,0)/N$. Normalized to $\psi(0,0)$, the first winding (closest to $\phi = z = 0$) is on the contour $(1 - 1/2N)$, the second on $(1 - 3/2N)$, the third on $(1 - 5/2N)$, et cetera. In general then, the jth wire is to be placed on the contour given by the locus of points $\{\phi_j, z_j\}$ that satisfy

$$\frac{\psi(\phi_j, z_j)}{\psi(0,0)} = 1 - \frac{2j-1}{2N} \tag{13}$$

for all $0 \leqslant \phi_j \leqslant \pi/2$. The loci of points $\{\pm\phi_j, z_j\}$ in the first and fourth quadrant respectively combine to form closed current loops, as do $\{\pi \pm \phi_j,\ z_j\}$ in the third and second quadrants.

3. The magnetic field and shield currents of the cylindrical saddle-shaped coil

The geometry of the cylindrical saddle-shaped coil shown in Fig. 1 is defined by three parameters: l is the coil half-length, a is the radius of the cylinder on which the coil is wound, and φ is the angle that locates the axial current paths. Carrying a current I, the saddle-shaped coil forms the surface current:

$$\begin{aligned} F_z(\phi,z) = \frac{I}{a}[&-\delta(\phi+\pi-\varphi) - \delta(\phi+\varphi) + \delta(\phi-\varphi) \\ &+ \delta(\phi-\pi+\varphi)] \times [H(z+l) - H(z-l)], \end{aligned} \tag{14}$$

$$\begin{aligned} F_\phi(\phi,z) = I[&1 - H(\phi+\pi-\varphi) - H(\phi+\varphi) + H(\phi-\varphi) \\ &+ H(\phi-\pi+\varphi)] \times [-\delta(z+l) + \delta(z-l)], \end{aligned} \tag{15}$$

where $H(\zeta)$ is the Heaviside step function. Substitution into Eq. (2) gives the Fourier components of the coil surface current:

[3] An exception arises for the case of an infinitely long straight wire. This issue is discussed in Appendix B.

$$F_z^m(k) = \frac{-\mathrm{i}4I}{\pi ka}\sin kl \sin m\varphi \;\delta_{m,\mathrm{odd}}, \tag{16}$$

$$F_\phi^m(k) = \frac{\mathrm{i}4I}{\pi m}\sin kl \sin m\varphi \;\delta_{m,\mathrm{odd}}, \tag{17}$$

which, via Eqs. (7) and (8), give:

$$f_z^m(k) = \frac{\mathrm{i}4Ia}{\pi kb^2}\frac{I'_m(ka)}{I'_m(kb)}\sin kl \sin m\varphi \;\delta_{m,\mathrm{odd}}, \tag{18}$$

$$f_\phi^m(k) = \frac{-\mathrm{i}4Ia}{\pi mb}\frac{I'_m(ka)}{I'_m(kb)}\sin kl \sin m\varphi \;\delta_{m,\mathrm{odd}}, \tag{19}$$

the Fourier components of the surface current on $\rho = b > a$ required to perfectly shield the coil.

The total magnetic field of the coil and shield is found by substitution of Eqs. (16) and (18) into Eq. (4). It is identically zero for all $\rho > b$. In the region $\rho < a$, interior to the coil, the field components are

$$\begin{pmatrix} B_\rho \\ B_\phi \\ B_z \end{pmatrix} = \frac{8\mu_o Ia}{\pi^2}\sum_{m=1,3,5,\ldots}^{\infty}\sin m\varphi \int_0^\infty \mathrm{d}k \,\sin kl \times \left[K'_m(ka) - \frac{I'_m(ka)}{I'_m(kb)}K'_m(kb)\right] \times \begin{pmatrix} \frac{-k}{m}\cos m\phi\cos kz\; I'_m(k\rho) \\ \frac{1}{\rho}\sin m\phi\cos kz\; I_m(k\rho) \\ \frac{k}{m}\cos m\phi\sin kz\; I_m(k\rho) \end{pmatrix}. \tag{20}$$

On the central axis of the coil, B_z vanishes—which is evident by symmetry—and only the $m = 1$ term survives[4] in the expressions for B_ρ and B_ϕ. At the isocenter of coil, with $\phi = 0$, the magnetic field has only the radial component

$$B_\rho(0,0,0) = B_c\left\{\frac{\lambda(2+\lambda^2)}{(1+\lambda^2)^{3/2}} + \frac{2}{\pi}\int_0^\infty \mathrm{d}\kappa\,\kappa \sin\kappa\lambda \frac{I'_1(\kappa)}{I'_1(\kappa\beta)}K'_1(\kappa\beta)\right\}, \tag{21}$$

where $B_c = 2\mu_o I\sin\varphi/(\pi a)$ and the dimensionless parameters are $\lambda = l/a$, $\beta = b/a$, and $\kappa = ka$. The first term in Eq. (21) is the contribution from the coil and agrees with the result given by Ginsberg and Melchner (see Eq. (1) of [15]); the second term is the contribution from the shield, which leads to a reduction of the total magnetic field inside the coil. In the limit that the aspect ratio l/a (i.e., λ) of the coil is large, Eq. (21) reduces to

$$B_\rho^\infty(0,0,0) = B_c\left\{1 - \frac{1}{\beta^2}\right\}, \tag{22}$$

which is independent of λ. This asymptotic behaviour is apparent in the plot of $B_\rho(0,0,0)$ versus λ shown in Fig. 2.

[4] In the limit $\rho \to 0$, the modified Bessel function $I_m(k\rho) \to (k\rho/2)^m/m!$ and its derivative $I'_m(k\rho) \to \frac{1}{2}(k\rho/2)^{m-1}/(m-1)!$ for $m > 0$.

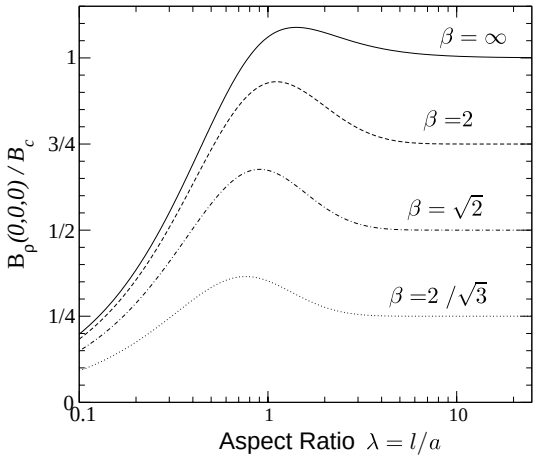

Fig. 2. The normalized magnetic field at the isocenter of the shielded saddle-shaped coil as a function of λ plotted for various β. The field strength is independent of λ when $\lambda \gg 1$. The contribution from azimuthal current paths leads to a peak in $B_\rho(0,0,0)$; for $\beta = \infty$ (unshielded coil) this occurs when $\lambda = \sqrt{2}$.

The homogeneity of the magnetic field produced by the cylindrical saddle-shaped coil can be optimized by eliminating all second derivatives of the field at the isocenter [15]. An alternative approach, suitable in many cases, is to require that only the second derivative of the transverse component $\partial^2 B_\rho(\rho,0,0)/\partial\rho^2$ vanishes. For the shielded coil, this leads to the relationship

$$9\sin\varphi\int_0^\infty \mathrm{d}\kappa\,\kappa^3\sin\kappa\lambda\left[K'_1(\kappa) - \frac{I'_1(\kappa)}{I'_1(\kappa\beta)}K'_1(\kappa\beta)\right] = -\sin 3\varphi\int_0^\infty \mathrm{d}\kappa\,\kappa^3\sin\kappa\lambda\left[K'_3(\kappa) - \frac{I'_3(\kappa)}{I'_3(\kappa\beta)}K'_3(\kappa\beta)\right], \tag{23}$$

which can be solved numerically for one of the parameters φ, λ, or β provided the other two are given. Fig. 3 shows a plot of φ^{opt}—the angle φ that satisfies Eq. (23)—as a function of λ and β. In the limit $\lambda \to \infty$, $\varphi^{\mathrm{opt}} = 60°$ independent of the proximity of the shield to the coil.

We further note that Eq. (23) reduces to

$$9(\lambda^2 - 4)\sin\varphi = (20 + 35\lambda^2 + 28\lambda^4 + 8\lambda^6)\sin 3\varphi \tag{24}$$

for $\beta = \infty$ (the unshielded coil), and that the same constraint is found by setting Eq. (3) from Ginsberg and Melchner [15] to zero. Their result that $\varphi^{\mathrm{opt}} = 60°$ for $\lambda = 2$ is evident from Eq. (24). For a coil with $\lambda = 1.6554$, we find $\varphi^{\mathrm{opt}} = 60.384°$ which is consistent with the value $\varphi^{\mathrm{opt}} = 60.38°$ quoted by Abel et al. [14]. Both of these coil configurations are indicated on the $\beta = \infty$ curve in Fig. 3.

Returning our attention to the active shielding of cylindrical saddle-shaped coils, the inverse transform of Eqs. (18) and (19) gives

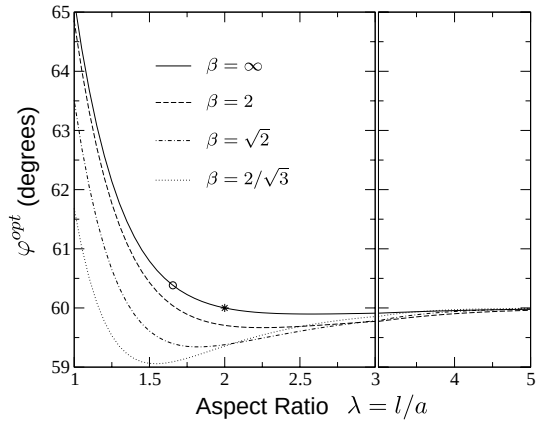

Fig. 3. The angular position φ^{opt} of the axial current paths that optimize the magnetic field homogeneity of a shielded saddle-shaped coil. When $\lambda \gg 1$, $\varphi^{\text{opt}} = 60°$ independent of β. The configuration of the unshielded coil noted by Abel et al. [14] is indicated by the circle. For the well known configuration ($\varphi^{\text{opt}} = 60°$, $\lambda = 2$), indicated by the asterisk, all second derivatives of the field are zero at the isocenter [15,16].

$$f_z(\phi,z) = \frac{-8Ia}{\pi^2 b^2} \sum_{m=1,3,5\ldots}^{\infty} \sin m\phi \sin m\varphi \times \int_0^{\infty} \mathrm{d}k \, \frac{\cos kz \sin kl}{k} \frac{I'_m(ka)}{I'_m(kb)}, \tag{25}$$

$$f_\phi(\phi,z) = \frac{8Ia}{\pi^2 b} \sum_{m=1,3,5\ldots}^{\infty} \frac{\cos m\phi \sin m\varphi}{m} \times \int_0^{\infty} \mathrm{d}k \, \sin kz \sin kl \frac{I'_m(ka)}{I'_m(kb)} \tag{26}$$

for the components of the shield surface current on $\rho = b$. These equations give the eddy-current distribution that would be induced on a passive shield, e.g., a highly conducting metallic cylinder that is very long compared to the coil. To approximate this distribution using the discrete line currents of an active shield, one makes use of the stream function

$$\psi(\phi,z) = \frac{-8Ia}{\pi^2 b} \sum_{m=1,3,5\ldots}^{\infty} \frac{\cos m\phi \sin m\varphi}{m} \times \int_0^{\infty} \mathrm{d}k \, \frac{\cos kz \sin kl}{k} \frac{I'_m(ka)}{I'_m(kb)}, \tag{27}$$

found by integrating either Eq. (25) or Eq. (26) as described in Section 2.3. Evenly spaced contours of Eq. (27) give the wire positions in the shield. An example is discussed in Section 4.2.

3.1. The infinitely long saddle-shaped coil: 2D description

While in practice the construction of very long coils is rarely of interest, one should be familiar with the 2D magnetic field profile of the infinitely long current structure since it provides a very useful conceptual tool for coil design. The pertinent results can be derived from those of the preceding section recognizing that $\sin kl/(\pi k) \to \delta(k)$ in the limit $l \to \infty$.

Alternatively, one may begin with the surface current of the infinitely long, saddle-shaped coil

$$F_z(\phi) = \frac{I}{a}[-\delta(\phi + \pi - \varphi) - \delta(\phi + \varphi) + \delta(\phi - \varphi) + \delta(\phi - \pi + \varphi)], \tag{28}$$

which has the Fourier transform

$$F_z^m(k) = -\mathrm{i}\frac{4I}{a} \sin m\varphi \, \delta_{m,\text{odd}} \, \delta(k) \tag{29}$$

and which, in turn, leads to

$$f_z^m(k) = \mathrm{i}\frac{4I}{b} \sin m\varphi \left(\frac{a}{b}\right)^{|m|} \delta_{m,\text{odd}} \, \delta(k) \tag{30}$$

for the Fourier transform of the shield surface current on $\rho = b$. Substitution of the latter two equations into Eq. (4) gives the total magnetic field, which, in the region $\rho < a$, is

$$\begin{pmatrix} B_\rho \\ B_\phi \end{pmatrix} = \frac{2\mu_o I}{\pi a} \sum_{m=1,3,5\ldots}^{\infty} \sin m\varphi (\rho/a)^{m-1} \times \left[1 - (a/b)^{2m}\right] \begin{pmatrix} \cos m\phi \\ -\sin m\phi \end{pmatrix}. \tag{31}$$

The first term in square braces is due to the coil and can be verified using the well-known result for the magnetic field due to a long straight wire (see Appendix C). On the central axis, with $\phi = 0$, Eq. (31) reduces to Eq. (22).

Finally, the inverse transform of Eq. (30) gives the shield surface current for the infinitely long coil

$$f_z(\phi) = \frac{-4I}{\pi b} \sum_{m=1,3,5\ldots}^{\infty} \sin m\phi \sin m\varphi \left(\frac{a}{b}\right)^m \tag{32}$$

with

$$\psi(\phi) = \frac{-4I}{\pi} \sum_{m=1,3,5\ldots}^{\infty} \frac{\cos m\phi \sin m\varphi}{m} \left(\frac{a}{b}\right)^m \tag{33}$$

being the associated stream function.

4. Examples

4.1. Reducing RF power deposition on a cryostat

The efficacy of an active shield improves with the number of discrete currents used to approximate the ideal shield surface current. To demonstrate this we consider the use of an active shield to reduce the power deposited on the inner surface of a conducting cylindrical surface due to the oscillating magnetic field of an inner transmit coil. This situation may occur in a low temperature NMR experiment where the apparatus is contained within a cylindrical metallic cryostat. Here

RF-pulses from an unshielded transmit coil will induce eddy currents on the cryostat that may adversely affect its intended performance. Under such circumstances it would be desirable to decouple the coil from the cryostat using an actively driven shield.

To explore this quantitatively, we calculate the power deposited on a conducting cylindrical surface $\rho = c$ due to a transmit coil at $\rho = a < c$ as a function of the number of current elements in an active shield that is situated between the two at $\rho = b$. We use radii of ratio $a{:}b{:}c = 2{:}3{:}4$, and, for simplicity, take all three structures to be infinitely long. The geometry of the problem is shown in the inset of Fig. 4. For the purpose of this demonstration, the transmit coil is taken to be a single-turn saddle-shaped coil with optimal angle $\varphi = 60°$. The active shield comprises N saddle-shaped coil elements each of angle φ_j determined using the appropriate stream function.

To begin we note that the surface current induced on the cylinder is calculated using Eq. (32). The contribution due to the transmit coil is

$$f_{cc}(\phi) = \frac{-2I_c}{\pi a} \sum_{m=1,5,7\ldots}^{\infty} \sin m\phi \sin(m\pi/3) \left(\frac{1}{2}\right)^m \tag{34}$$

with the summation being over odd values of m not equal to a multiple of 3. The contribution due to the shield is

$$f_{cs}(\phi) = \sum_{j=1}^{N} \frac{-2I_s}{\pi a} \sum_{m=1,3,5\ldots}^{\infty} \sin m\phi \sin m\varphi_j \left(\frac{3}{4}\right)^m. \tag{35}$$

The current I_s and angles φ_j are determined for a given value of N through the the use of the stream function

$$\psi_s(\phi) = \frac{-4I_c}{\pi} \sum_{m=1,5,7\ldots}^{\infty} \frac{\cos m\phi \sin m\pi/3}{m} \left(\frac{2}{3}\right)^m \tag{36}$$

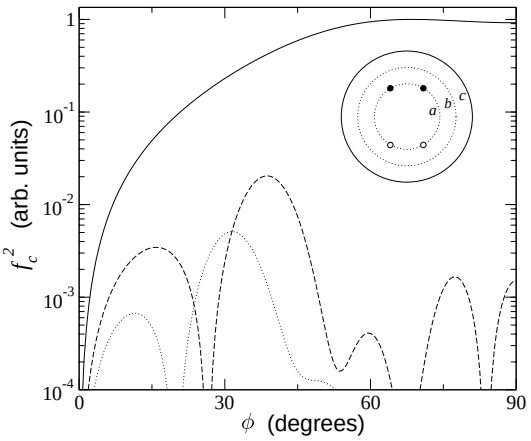

Fig. 4. Square of the induced surface current on cylinder due to inner transmit coil. Results are shown for the case with no shield, $N = 0$ (solid line), as well as for shields comprising $N = 3$ (dashed line) and $N = 5$ (dotted line) coil elements. Inset diagram: transmit coil on $\rho = a$; active shield constructed on $\rho = b$; conducting metallic cylinder on $\rho = c$.

Table 1
Configuration and efficacy of the active shield

N	φ_j (degrees)	η	P
0	—	1	1
2	46.1, 72.9	1.368	0.022
3	39.5, 60, 78.1	1.361	0.0060
4	35.2, 53.7, 66.2, 80.9	1.358	0.0026
5	32.0, 49.4, 60, 70.1, 82.6	1.356	0.0013

The shield comprises N coil elements, whose positions are given by the angles φ_j. The normalized current η is required for a standard magnetic field. The efficacy of the shield is characterized by P, the total power per unit length deposited on the cylinder normalized to the unshielded case ($N = 0$).

associated with the surface current on $\rho = b$ that would perfectly shield the transmit coil. From Eq. (12), the current to be carried by each of the N coil elements in the shield is $I_s = \psi_s(0)/N$, which evaluates to $-0.715 \times I_c/N$ in this example. The angular position of the jth coil in the shield is found by satisfying the condition of Eq. (13). Table 1 gives all φ_j for $N = 2$ to 5.

The magnetic field B_{cc} (B_{cs}) due to the coil (shield) and its induced surface current on the cylinder are found using Eq. (31). The total magnetic field on the axis is

$$\begin{aligned} B_c &= B_{cc}(0,0) + B_{cs}(0,0) \\ &= \frac{\mu_o I_c}{\pi a} \left\{ \frac{3\sqrt{3}}{4} - 0.715 \times \frac{7}{12N} \sum_{j=1}^{N} \sin \varphi_j \right\}. \end{aligned} \tag{37}$$

To properly determine the efficacy of the shield, we must ensure that the field B_c is the same for any given N. This requires that the current I_c be multiplied by the factor

$$\eta = \frac{B_{cc}(0,0)}{B_{cc}(0,0) + B_{cs}(0,0)} \tag{38}$$

that depends on the number of coil elements used in the shield. Values of η are given in Table 1; note that in the limit $N \to \infty$, the ideal shield surface current exists on $\rho = b$ and $\eta \to 1.35$ exactly.

The power per unit length deposited on the cylinder is proportional to

$$f_c^2 = \eta^2 (f_{cc} + f_{cb})^2 \tag{39}$$

which is the square of the total induced surface current. This is plotted as a function of angle in Fig. 4 for various N to highlight the effect of shielding. The total integrated power (the area under the curve f_c^2) is given in Table 1 normalized to the unshielded case. A shield with $N = 2$ is sufficient to reduce the power deposited on the cylinder to ~2%; doubling the number of elements in the shield to $N = 4$ further reduces the absorbed power by an order of magnitude.

4.2. Transmit coil for very low field MRI

Magnetic resonance imaging of the human body requires a transverse B_1 field that is uniform over a large

volume. One approach that can be taken to minimize the design constraints on low-frequency RF systems is to use separate transmit and receive coils. This allows one to increase the size of the transmit coil for better homogeneity without an accompanying reduction in the filling factor on the receive end [1]. This approach has been used recently in very low field NMR and MRI measurements of ^{3}He in the human lung [4,5]. In that work, an unshielded wire-wound transmit coil, separate from a detection coil system, was designed to generate RF-pulses uniform to within 5% over a volume comparable to the human lung space ($\Delta x = \Delta z = 2\Delta y = \pm 15$ cm from coil isocenter). The field homogeneity of this coil was sufficient to re-focus thousands of ^{3}He spin-echoes with negligible π-pulse losses [5].

Here we demonstrate that a transmit coil of comparable quality can be readily designed from a reasonable number of saddle-shaped current elements. We choose $M = 5$ elements as a practical number. We examine two coil designs of different aspect ratio, $l/a = 2$ and 1.5, and in both cases take $a = 22.5$ cm as a suitable radius for a human-sized coil. The five current elements are to be driven in series and are assumed to be operated at sufficiently low frequency that the current I is everywhere in-phase.[5] For simplicity, the angular positions of the five elements ($\varphi_j = \{25.8°, 45.6°, 60°, 72.5°, 84.3°\}$) were determined from the stream function of the sine–phi surface current distribution (see Appendix D), which is equivalent to using a target field approach [7,12,24] with a target field homogeneous over $\rho < a$ and independent of z.

The transverse component of the magnetic field

$$B_x = B_\rho \cos\phi - B_\phi \sin\phi \tag{40}$$

is calculated for the saddle-shaped current element using Eqs. (16) and (4) with $f_z^m(k) = 0$. In the central plane ($\phi = 0$), the internal transverse field produced by a coil of M series driven elements is

$$B_x = \frac{-8\mu_o Ia}{\pi^2} \sum_{j=1}^{M} \sum_{m=1,3,5,\ldots}^{\infty} \frac{\sin m\varphi_j}{m} \int_0^\infty \mathrm{d}k\, k \sin k l_j \times \cos kz\, K'_m(ka) I'_m(kx), \tag{41}$$

where in general the length l_j of each element may be different. We use this equation to compute field maps for the two transmit coil designs considered here. The results are shown in Fig. 5; both designs offer very good field homogeneity, with the longer coil being the better of the two.

[5] Note that such coils produce a linearly polarized magnetic field and therefore are not necessarily as efficient as a resonator for spin rotation [8].

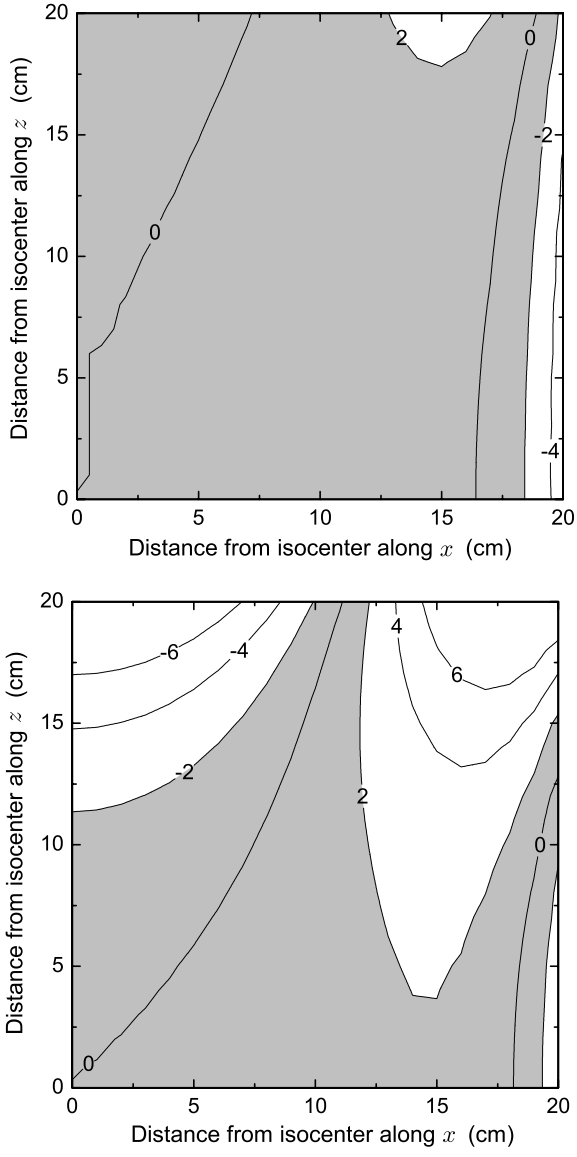

Fig. 5. Contour map of the transverse magnetic field (as a percent difference from the central field) for the coil of half-length $l = 2a$ (top) and $1.5a$ (bottom). The shaded regions (±2%) highlight differences between the two geometries.

4.2.1. A series-driven active shield using saddle-shaped current elements

In general, the integrated value of the ideal shield surface current (Eq. (25) into Eq. (12)) for a saddle-shaped current element is always $I_s = -pI$, where $p \leqslant 1$ and depends on the shield radius b. Notice then that for a transmit coil comprising M saddle-shaped current elements and total integrated current MI, it is possible to choose b such that $p = N/M$ is a rational number; and a shield can thus be constructed using an integer $N < M$ current elements (not forcibly saddle-shaped as will be seen). Also notice that such a configuration is extremely convenient to use, since the shield can be driven in series with the transmit coil using the same current source.

To determine b for a chosen N, one makes use of the stream function

$$\psi_s(\phi,z) = \frac{-8Ia}{\pi^2 b}\sum_{j=1}^{M}\sum_{m=1,3,5\ldots}^{\infty}\frac{\cos m\phi \sin m\varphi_j}{m} \times \int_0^\infty \mathrm{d}k \frac{\cos kz \sin kl_j}{k}\frac{I'_m(ka)}{I'_m(kb)}, \quad (42)$$

which comes from Eq. (27); conjugate values of b and N satisfy the condition $I_s = -NI$ where $I_s = \psi_s(0,0)$. For example, a series-driven active shield for the long transmit coil mentioned above can be constructed with $N = 4$ current elements on the radius $b = 27.9$ cm. The current elements are placed on the equispaced contours of the stream function which are given by the loci of points $\{\phi_j, z_j\}$ found using Eq. (42) in Eq. (13). These are shown in Fig. 6 along with a contour plot of the shield surface current,[6] which is found by substitution of Eq. (42) into Eq. (11). One can see that a closer physical spacing of the stream function contours corresponds to a higher value of the shield surface current.

For ease of construction, one may choose to make a further approximation and use saddle-shaped current elements for the shield, as shown in Fig. 6. This has the added advantage that one can readily calculate the magnetic field contribution from the shield using the expressions given in this paper. For example, B_x is calculated using the appropriate form of Eq. (41), and plots of the transverse field produced by the shielded and unshielded coil are shown in Fig. 7.

4.2.2. Further considerations

The coil designs discussed above are suitable for generating very homogeneous tipping pulses over a volume comparable to that of the human lungs. These designs were based on the ideal sine–phi surface current distribution and have not been optimized further with respect to finite length. However, with the expressions for the magnetic field of the saddle-shaped current element developed in this paper, one can readily explore the limited parameter space (φ_j and l_j for a given coil radius) to optimize quantities such as field homogeneity or shielding. One might also choose to use the magnetic field of the sine–phi distribution, appropriately apodized over z, as a target field [7,12,24] to generate more complex winding patterns with potentially improved field characteristics. Of course, as suggested above, one might still opt to approximate these winding patterns with saddle-shaped elements to take advantage of their ease of construction and the well-defined expressions for $\boldsymbol{B}$ given here.

The most straightforward way to improve both the homogeneity and shielding of a coil is to simply increase the number of saddle-shaped current elements used in its construction. One should keep the following in mind if proceeding in this direction. First, as the number of

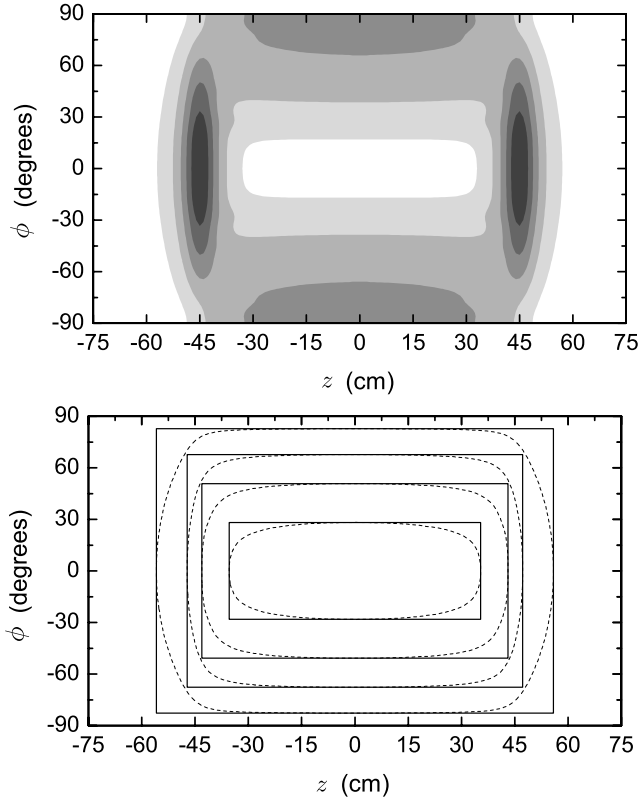

Fig. 6. Top panel: Contour plot of the surface current required to perfectly shield the long transmit coil of Fig. 5. Only the region $z = \pm 75$ cm is shown. Darker shading indicates a higher value. Bottom panel: four equispaced stream function contours (dashed lines). Their positions along $z = 0$ and $\phi = 0$ (i.e., $\varphi_j = \{28.2°, 50.8°, 67.7°, 82.7°\}$ and $l_j = \{35.4, 43.1,\ 47.2, 55.9\}$ cm) define four saddle-shaped current elements (solid lines).

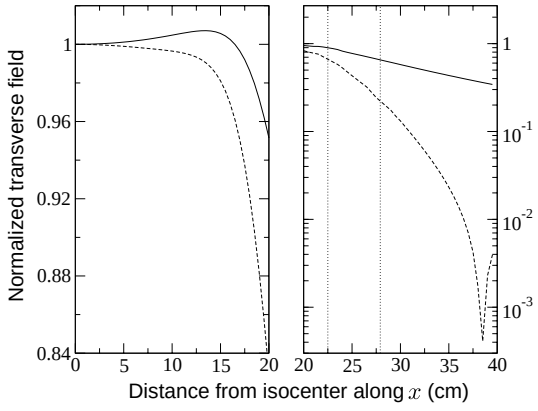

Fig. 7. Normalized transverse field $|B_x(x,0,0)/B_x(0,0,0)|$ for the unshielded (solid line) and shielded (dashed line) long transmit coil of Fig. 5. Left panel: the field inside the coil. Homogeneity is preserved for $x < 15$ cm. Right panel: the field beyond $x = 20$ cm. The vertical dotted lines indicate the coil and shield radii. At $x = 38.5$ cm the field changes sign indicating that the shield begins to overcompensate at this point.

[6] Note that the stream function, like the shield surface current, tends to zero as $z \to \pm\infty$ and that no truncation of this function is required to constrain the position of the outermost current element.

current elements is increased, so do the self-inductance and capacitance of the coil which lowers its self-resonance and limits its usable frequency range. Second, the length of the contiguous wire used to construct the coil may become comparable to the wavelength of light at the desired operating frequency. Under such conditions, the assumption that the current is in-phase throughout the coil will not be met and calculated field profiles will not be accurate. This effect may have contributed to a slight asymmetry (<0.5%) observed in the homogeneity of a transmit coil previously designed and built for very low field MRI [26].

5. Summary

In this paper, we have considered the use of the cylindrical saddle-shaped coil as the building-block for the construction of wire-wound RF coils with active shields. We have attempted to supply a complete set of mathematical and conceptual tools for this purpose, and have striven to demonstrate their utility with the examples provided. In particular, expressions for the magnetic field produced by the saddle-shaped coil and the stream function associated with its ideal shield surface current should prove very useful for the design of actively shielded low-frequency RF coils. Shielded transmit coils offer a homogeneous B_1 field unperturbed by induced currents in external structures; likewise, by the principle of reciprocity [16], shielded receive coils offer a uniform sensitivity to the sample signal decoupled from external fields. Such coils should find application in very low field NMR and MRI, where RF resonators become difficult to operate and passive shielding techniques interfere with the production of switched gradient fields. The results of Section 3 are also useful for the calculation of eddy currents induced on cylindrical metallic enclosures by saddle-shaped coils, as well as for the determination of the total magnetic field produced by the two.

Acknowledgments

We gratefully acknowledge the support of the Natural Sciences and Engineering Research Council of Canada and the British Columbia Advanced Systems Institute. We thank C.V. Kaiser, G. Archibald, and B.W. Filippone for helpful discussions.

Appendix A. The magnetic field produced by a cylindrically constrained surface current

A general current density $\boldsymbol{J}$ confined to flow on a cylindrical surface $\rho = s$ is shown in Fig. 8 and is described by Eq. (1) of Section 2. Since there is no radial

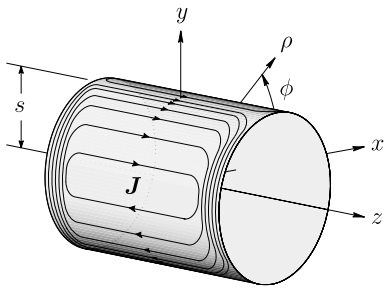

Fig. 8. Current flow constrained to a cylindrical surface $\rho = s$.

current flow, the components of the vector potential $\boldsymbol{A}$ at the point $\boldsymbol{r}$ are

$$\begin{pmatrix} A_\rho \\ A_\phi \\ A_z \end{pmatrix} = \frac{\mu_o}{4\pi} \int \frac{\mathrm{d}v'}{|\boldsymbol{r}-\boldsymbol{r}'|} \begin{pmatrix} J_\phi(\boldsymbol{r}')\sin(\phi-\phi') \\ J_\phi(\boldsymbol{r}')\cos(\phi-\phi') \\ J_z(\boldsymbol{r}') \end{pmatrix}, \tag{A.1}$$

where $J_\phi(J_z)$ is the azimuthal (axial) component of the current density at the point $\boldsymbol{r}'$. The integration is over the primed coordinates with volume element $\mathrm{d}v' = \rho'\,\mathrm{d}\rho'\,\mathrm{d}\phi'\,\mathrm{d}z'$.

In cylindrical coordinates, this equation can be expanded using the Green function

$$\frac{1}{|\boldsymbol{r}-\boldsymbol{r}'|} = \frac{2}{\pi}\sum_{m=-\infty}^{\infty} \mathrm{e}^{\mathrm{i}m(\phi-\phi')} \int_0^\infty \mathrm{d}k \cos k(z-z') I_m(k\rho^<) K_m(k\rho^>), \tag{A.2}$$

where $I_m(K_m)$ is the modified Bessel function of the first (second) kind and $\rho^<(\rho^>)$ is the smaller (larger) of ρ and ρ' [23]. Following the approach of Turner and Bowley [11], however, a more compact notation is achieved[7] if one uses the definition

$$\frac{1}{|\boldsymbol{r}-\boldsymbol{r}'|} = \frac{1}{\pi}\sum_{m=-\infty}^{\infty} \mathrm{e}^{\mathrm{i}m(\phi-\phi')} \int_{-\infty}^\infty \mathrm{d}k\, \mathrm{e}^{\mathrm{i}k(z-z')} I_m(k\rho^<) K_m(k\rho^>). \tag{A.3}$$

Integrating Eq. (A.1) over ρ' and making use of Eq. (A.3) gives

$$\begin{pmatrix} A_\rho \\ A_\phi \\ A_z \end{pmatrix} = \frac{\mu_o s}{4\pi} \sum_{m=-\infty}^{\infty} \mathrm{e}^{\mathrm{i}m\phi} \int_{-\infty}^\infty \mathrm{d}k\, \mathrm{e}^{\mathrm{i}kz} \times \begin{pmatrix} -\mathrm{i}[G_{m-1}(s) - G_{m+1}(s)]F_\phi^m(k) \\ [G_{m-1}(s) + G_{m+1}(s)]F_\phi^m(k) \\ 2G_m(s)F_z^m(k) \end{pmatrix}, \tag{A.4}$$

[7] This comes at the expense of possibly introducing confusion over how to handle the integration over $K_m(\zeta)$ which is complex for real $\zeta < 0$ [27]. A re-analysis of Appendix A using the Green function of Eq. (A.2) shows, by way of comparison, that only the real term of $K_m(-\zeta)$ is physically meaningful. As a result, one may treat $K_m(-\zeta)$ as $(-1)^m K_m(\zeta)$—and $K'_m(-\zeta)$ as $-(-1)^m K'_m(\zeta)$—for the purposes of this and related articles.

where

$$G_m(s) = \begin{cases} I_m(k\rho)K_m(ks), & \text{when } \rho < s \\ I_m(ks)K_m(k\rho), & \text{when } \rho > s \end{cases} \tag{A.5}$$

and $F^m_\phi(k)$ and $F^m_z(k)$ are defined in Eq. (2).

The magnetic field $\boldsymbol{B} = \nabla \times \boldsymbol{A}$ is calculated from Eq. (A.4) using the appropriate form of the curl operator. For the radial component of $\boldsymbol{B}$ this gives

$$B_\rho = \frac{\mu_o s}{4\pi \mathrm{i}} \sum_{m=-\infty}^{\infty} \mathrm{e}^{\mathrm{i}m\phi} \int_{-\infty}^{\infty} \mathrm{d}k\, \mathrm{e}^{\mathrm{i}kz} \times \left[k(G_{m-1}(s) + G_{m+1}(s))F^m_\phi(k) - \frac{2m}{\rho} G_m(s) F^m_z(k) \right] \tag{A.6}$$

which can be simplified by first substituting for $F^m_\phi(k)$ from Eq. (3) and then making use of the identity

$$-2I'_m(\zeta_1)K'_m(\zeta_2) = I_{m-1}(\zeta_1)K_{m-1}(\zeta_2) + I_{m+1}(\zeta_1)K_{m+1}(\zeta_2) + \frac{2m^2}{\zeta_1\zeta_2} I_m(\zeta_1)K_m(\zeta_2) \tag{A.7}$$

given in [11]. The result is

$$B_\rho = \frac{\mu_o s^2}{2\pi} \sum_{m=-\infty}^{\infty} \mathrm{e}^{\mathrm{i}m\phi} \int_{-\infty}^{\infty} \mathrm{d}k\, \mathrm{e}^{\mathrm{i}kz} \frac{k^2}{\mathrm{i}m} P_m(s) F^m_z(k), \tag{A.8}$$

where the function $P_m(s)$ is defined in Eq. (5).

Similar compact forms are found for the azimuthal and axial field components and are stated here for completeness:

$$B_\phi = \frac{\mu_o s^2}{2\pi} \sum_{m=-\infty}^{\infty} \mathrm{e}^{\mathrm{i}m\phi} \int_{-\infty}^{\infty} \mathrm{d}k\, \mathrm{e}^{\mathrm{i}kz} \frac{k}{\rho} Q_m(s) F^m_z(k), \tag{A.9}$$

$$B_z = \frac{\mu_o s^2}{2\pi} \sum_{m=-\infty}^{\infty} \mathrm{e}^{\mathrm{i}m\phi} \int_{-\infty}^{\infty} \mathrm{d}k\, \mathrm{e}^{\mathrm{i}kz} \frac{k^2}{m} Q_m(s) F^m_z(k), \tag{A.10}$$

where the function $Q_m(s)$ is defined in Eq. (6). The derivations make use of the identities

$$\frac{2I_m(\zeta_1)K'_m(\zeta_2)}{\zeta_1} + \frac{2I'_m(\zeta_1)K_m(\zeta_2)}{\zeta_2} = \frac{-1}{m}\left(I_{m-1}(\zeta_1)K_{m-1}(\zeta_2) - I_{m+1}(\zeta_1)K_{m+1}(\zeta_2)\right), \tag{A.11}$$

$$-2I_m(\zeta_1)K'_m(\zeta_2) = \frac{1-m}{\zeta_1} I_{m-1}(\zeta_1)K_{m-1}(\zeta_2) + \frac{1+m}{\zeta_1} I_{m+1}(\zeta_1)K_{m+1}(\zeta_2) + I'_{m-1}(\zeta_1)K_{m-1}(\zeta_2) + I'_{m+1}(\zeta_1)K_{m+1}(\zeta_2), \tag{A.12}$$

$$-2I'_m(\zeta_1)K_m(\zeta_2) = \frac{1-m}{\zeta_2} I_{m-1}(\zeta_1)K_{m-1}(\zeta_2) + \frac{1+m}{\zeta_2} I_{m+1}(\zeta_1)K_{m+1}(\zeta_2) + I_{m-1}(\zeta_1)K'_{m-1}(\zeta_2) + I_{m+1}(\zeta_1)K'_{m+1}(\zeta_2), \tag{A.13}$$

which can be derived from the recurrence formulae for modified Bessel functions.

Appendix B. Shielding 2D magnetic fields

A purely azimuthal or axial current will give rise to a magnetic field that is a function of two spatial variables only: ρ and z in the former case, and ρ and ϕ in the latter. If the current is continuous, with no charge accumulation, then the magnetic field is still given by Eq. (4) and the shielding conditions by Eqs. (7) and (8). These expressions are not valid, however, if there is a charge source/sink at infinity, such as in the case of the infinitely long wire.

To see this consider the surface current $\boldsymbol{F} = F_z(\phi)\boldsymbol{e}_z$ extending to $z = \pm\infty$ on $\rho = a$. With no azimuthal component and F_z independent of z, its Fourier transform is simply

$$F^m_\phi(k) = 0, \tag{B.1}$$

$$F^m_z(k) = F^m_z\,\delta(k) \tag{B.2}$$

with components F^m_z independent of k. We now seek the surface current $\boldsymbol{f} = f_z(\phi)\boldsymbol{e}_z$ on $\rho = b > a$ that will perfectly shield the magnetic field due to $\boldsymbol{F}$. Making use of Eq. (A.4), the total vector potential in the region $\rho > b$ is

$$A_z = \frac{\mu_o}{2\pi} \sum_{m=-\infty}^{\infty} \mathrm{e}^{\mathrm{i}m\phi} \times \int_{-\infty}^{\infty} \mathrm{d}k\, \mathrm{e}^{\mathrm{i}kz} K_m(k\rho)\left[aI_m(ka)F^m_z(k) + bI_m(kb)f^m_z(k)\right], \tag{B.3}$$

which vanishes when

$$f^m_z(k) = -\frac{aI_m(ka)}{bI_m(kb)} F^m_z(k) \tag{B.4}$$

is satisfied. This condition is only relevant for surface currents of the form described above. It can be simplified to

$$f^m_z(k) = -F^m_z\delta(k)(a/b)^{|m|+1} \tag{B.5}$$

by making use of Eq. (B.2). Note, however, that the substitution of Eq. (B.2) into the shielding condition of Eq. (7) gives

$$f^m_z(k) = -F^m_z\delta(k)\begin{cases} (a/b)^3, & m = 0, \\ (a/b)^{|m|+1}, & m \neq 0, \end{cases} \tag{B.6}$$

which results in an incorrect prefactor for the $f^0_z(k)$ term: $(a/b)^3$ instead of a/b. As a result, when the total axial current $aF^0_z = \int_{-\pi}^{\pi} a\ \mathrm{d}\phi\, F_z(\phi)$ is nonzero, the shield surface current must be determined from Eq. (B.5) and the magnetic field from Eq. (B.3).

An obvious illustration of this is the infinitely long wire. Carrying a current I and located at the position (a, φ), its surface current is

$$F_z(\phi) = (I/a)\delta(\phi - \varphi) \tag{B.7}$$

which has the Fourier transform

$$F_z^m(k) = (I/a)\exp(-\mathrm{i}m\varphi)\delta(k). \tag{B.8}$$

The surface current $f_z(\phi)$ on $\rho = b$ required for shielding is properly determined from Eq. (B.5) and found to be

$$f_z(\phi) = \frac{-I}{2\pi b}\left[1 + 2\sum_{m=1}^{\infty}\left(\frac{a}{b}\right)^m \cos m(\phi - \varphi)\right], \tag{B.9}$$

which correctly reduces to the surface current on a coaxial shield in the limit $a \to 0$.

Appendix C. The magnetic field of an infinitely long wire

In cylindrical coordinates, the magnetic field due to an infinitely long wire located at (a, φ) and carrying a current I is

$$\boldsymbol{B} = \frac{\mu_o I}{2\pi}\frac{-a\sin(\phi - \varphi)\boldsymbol{e}_\rho + (\rho - a\cos(\phi - \varphi))\boldsymbol{e}_\phi}{\rho^2 + a^2 - 2a\rho\cos(\phi - \varphi)}. \tag{C.1}$$

This well-known result can be rewritten using the identities [28]

$$\frac{r\sin\alpha}{1 - 2r\cos\alpha + r^2} = \sum_{m=1}^{\infty} r^m \sin m\alpha, \tag{C.2}$$

$$\frac{1 - r\cos\alpha}{1 - 2r\cos\alpha + r^2} = 1 + \sum_{m=1}^{\infty} r^m \cos m\alpha, \tag{C.3}$$

where $r < 1$. For $\rho < a$, the components of the magnetic field are

$$\begin{pmatrix} B_\rho \\ B_\phi \end{pmatrix} = \frac{-\mu_o I}{2\pi a}\sum_{m=1}^{\infty}(\rho/a)^{m-1}\begin{pmatrix} \sin m(\phi - \varphi) \\ \cos m(\phi - \varphi) \end{pmatrix}, \tag{C.4}$$

while for $\rho > a$, they are

$$\begin{pmatrix} B_\rho \\ B_\phi \end{pmatrix} = \frac{-\mu_o I}{2\pi\rho}\sum_{m=0}^{\infty}(a/\rho)^m\begin{pmatrix} \sin m(\phi - \varphi) \\ -\cos m(\phi - \varphi) \end{pmatrix}. \tag{C.5}$$

Notice that boundary conditions are satisfied at $\rho = a$: the perpendicular component B_ρ is continuous, while the tangential component B_ϕ is discontinuous by the amount

$$\frac{\mu_o I}{a}\frac{1}{2\pi}\sum_{m=-\infty}^{\infty}\cos m(\phi - \varphi) = \frac{\mu_o I}{a}\delta(\phi - \varphi) \tag{C.6}$$

due to the surface current $\boldsymbol{F}_z = I/a\ \delta(\phi - \varphi)\boldsymbol{e}_z$. Also note that Eqs. (C.4) and (C.5) can be derived using Eq. (B.8) and the expression for A_z from Eq. (A.4).

For the infinitely long saddle-shaped coil on $\rho = a$, with four wires located at $\pm\varphi$ and $\pm(\pi - \varphi)$ and carrying currents $\pm I$, the surface current is clearly that given by Eq. (28). Its magnetic field can be calculated in the region $\rho < a$ ($\rho > a$) by summing the contribution from each wire given by Eq. (C.4) (Eq. (C.5)).

Appendix D. The sine–phi surface current distribution

It is a commonly stated fact that a perfectly homogeneous transverse field can be generated inside a cylindrical volume using an infinitely long surface current of the form $\boldsymbol{F} \propto \sin\phi\,\boldsymbol{e}_z$ [1,7]. This sine–phi distribution forms the conceptual basis of transverse B_1 field generation; the construction of practical approximations to this distribution is the central endeavor of B_1 coil design.

One can derive the magnetic field produced by the sine–phi surface current distribution by solving the equivalent problem for the infinitely long cylinder with uniform transverse magnetization.[8] In keeping with the spirit of this paper, however, we follow the methods outlined in Section 2 and calculate the field from $\boldsymbol{F}$, including the contribution from an ideal shield surface current.

To begin, consider on $\rho = a$ the infinitely long surface current distribution

$$\boldsymbol{F} = F_o\ \sin\phi\ \boldsymbol{e}_z \tag{D.1}$$

which has Fourier components

$$F_z^m(k) = -\mathrm{i}m\pi F_o\delta(k)\delta_{m,\pm 1}. \tag{D.2}$$

From Eq. (7) the Fourier components of the shield surface current on $\rho = b$ are

$$f_z^m(k) = \mathrm{i}m\pi F_o\frac{a^2}{b^2}\delta(k)\delta_{m,\pm 1} \tag{D.3}$$

and making use of Eq. (9) one finds

$$\boldsymbol{f} = -(a/b)^2 F_o\sin\phi\ \boldsymbol{e}_z, \tag{D.4}$$

which is a also a sine–phi distribution. Substituting Eqs. (D.2) and (D.3) in Eq. (4) gives a complete description of the magnetic field:

[8] The magnetic field produced by an object of uniform magnetization $\boldsymbol{M}$ is identical to that due to a surface current $\boldsymbol{F} = \boldsymbol{M} \times \hat{\boldsymbol{n}}$, where $\hat{\boldsymbol{n}}$ is the unit vector normal to the surface of the object [25]. Here $\boldsymbol{B} = \mu_o(\boldsymbol{H} + \boldsymbol{M})$, and, in the absence of free charge, there exists a magnetic scalar potential Φ such that $\boldsymbol{H} = -\nabla\Phi$. For the transversely magnetized cylinder, $\boldsymbol{M} = M(\cos\phi\,\boldsymbol{e}_\rho - \sin\phi\,\boldsymbol{e}_\phi)$ from which one may glean that $\Phi \propto \rho\cos\phi$ inside the cylinder and $\rho^{-1}\cos\phi$ outside the cylinder. Satisfying boundary conditions completes the problem.

$$\boldsymbol{B} = \frac{\mu_o F_o}{2} \begin{cases} (1 - a^2/b^2)\left(\cos\phi\ \boldsymbol{e}_\rho - \sin\phi\, \boldsymbol{e}_\phi\right), & \rho < a, \\ a^2(\rho^{-2} - b^{-2})\cos\phi\ \boldsymbol{e}_\rho & \\ \quad + a^2(\rho^{-2} + b^{-2})\sin\phi\ \boldsymbol{e}_\phi, & a < \rho < b, \\ 0, & \rho > b. \end{cases} \tag{D.5}$$

In the region $\rho < a$, the field is perfectly homogeneous, directed parallel the vector $\hat{\boldsymbol{x}} = (\cos\phi\ \boldsymbol{e}_\rho - \sin\phi\ \boldsymbol{e}_\phi)$. And, as desired, it is everywhere zero for $\rho > b$.

D.1. Line current approximation to the sine–phi surface current

Consider approximating a sine–phi surface current distribution on $\rho = a$ with N infinitely long wires per quadrant. Owing to the symmetry of the problem the following calculations can be restricted to the first quadrant. From Eq. (D.1), the total integrated surface current on $\rho = a$ over the interval $\phi = 0$ to $\pi/2$ is aF_o. This area is divided into N equal parts—bound by $N + 1$ angles α_j, beginning with $\alpha_0 = 0$ and ending with $\alpha_N = \pi/2$—so that each wire carries an equivalent integrated surface current aF_o/N. The angular position φ_j of each wire is chosen to be the mid-point of the integrated surface current over the interval $[\alpha_{j-1}, \alpha_j]$ and satisfies the conditions

$$\int_{\alpha_{j-1}}^{\varphi_j} F_o \sin\phi\ a\ \mathrm{d}\phi = \int_{\varphi_j}^{\alpha_j} F_o \sin\phi\ a\ \mathrm{d}\phi = \frac{aF_o}{2N}. \tag{D.6}$$

From Eq. (D.6), a general formula for all wire positions is found

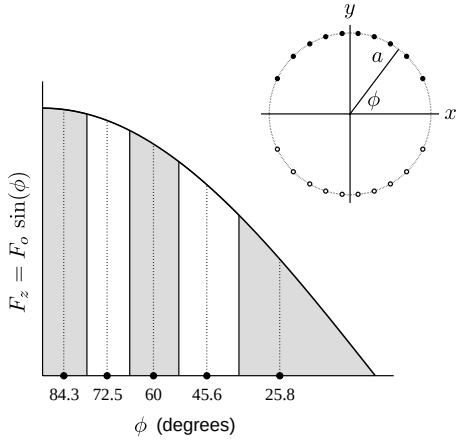

Fig. 9. Bottom-left: the sine–phi surface current distribution in the first quadrant and its approximation using $N = 5$ wires. Areas of equal integrated surface current are separated by solid lines (shading alternated for clarity); each area is divided in half (dashed line) and the corresponding angle sets the wire position (circle). Top-right: the cross-section of the associated winding pattern on $\rho = a$. The closed versus open circles indicate current flow in opposite directions.

$$\varphi_j = \arccos\left(1 - \frac{2j-1}{2N}\right), \tag{D.7}$$

which is equivalent to Eq. (13) noting that the stream function of the sine–phi distribution is $\psi(\phi) \propto \cos\phi$.

Eq. (D.7) is evaluated for $j = 1, \ldots, N$ only. The $4N$ wires that comprise the entire coil are located symmetrically with a wire at each $\pm\varphi_j$ and $\pm(180° - \varphi_j)$. For $N = 1$ the four wire positions are $\pm 60°$ and $\pm 120°$. The general principle is illustrated in Fig. 9 for the case $N = 5$.

References

[1] C.E. Hayes, W.A. Edelstein, J.F. Schenck, Radio frequency resonators, in: Magnetic Resonance Imaging, Chapter 72, 2nd ed., W.B. Saunders, Philadelphia, 1988, pp. 1183–1200.
[2] S.K. Lee, M. Mößle, W. Myers, N. Kelso, A.H. Trabesinger, A. Pines, J. Clarke, SQUID-detected MRI at 132 μT with T_1-weighted contrast established at 10 μT–300 mT, Magn. Reson. Med. 53 (2005) 9–14.
[3] A.N. Matlachov, P.L. Volegov, M.A. Espy, J.S. George, R.H. Kraus Jr., SQUID detected NMR in microtesla magnetic fields, J. Magn. Reson. 170 (2004) 1–7.
[4] C.P. Bidinosti, J. Choukeife, P.-J. Nacher, G. Tastevin, In vivo NMR of hyperpolarized ^{3}He in the human lung at very low magnetic fields, J. Magn. Reson. 162 (2003) 122–132.
[5] C.P. Bidinosti, J. Choukeife, G. Tastevin, A. Vignaud, P.-J. Nacher, MRI of the lung using hyperpolarized ^{3}He at very low magnetic field (3 mT), MAGMA 16 (2004) 255–258.
[6] M.E. Hayden, G. Archibald, K.M. Gilbert, C. Lei, Restricted diffusion within a single pore, J. Magn. Reson. 169 (2004) 313–322.
[7] J.-M. Jin, Electromagnetics in magnetic resonance imaging, IEEE Antennas Propagation Mag. 40 (1998) 7–22.
[8] C.E. Hayes, W.A. Edelstein, J.F. Schenck, O.M. Mueller, M. Eash, An efficient, highly homogeneous radiofrequency coil for whole-body NMR imaging at 1.5 T, J. Magn. Reson. 63 (1985) 622–628.
[9] D. Yeung, J.M.S. Hutchison, D.J. Lurie, An efficient birdcage resonator at 2.5 MHz using a novel multilayer self-capacitance construction technique, MAGMA 3 (1995) 163–168.
[10] P. Mansfield, B. Chapman, Active magnetic screening of coils for static and time-dependent magnetic field generation in NMR imaging, J. Phys. E 19 (1986) 540–545.
[11] R. Turner, R.M. Bowley, Passive screening of switched magnetic field gradients, J. Phys. E 19 (1986) 876–879.
[12] R. Turner, Gradient coil design-a review of methods, Magn. Reson. Imaging 11 (1993) 903–920.
[13] M.A. Brideson, L.K. Forbes, S. Crozier, Winding patterns for actively shielded shim coils with asymmetric target-fields, Meas. Sci. Technol. 14 (2003) 484–493.
[14] W.R. Abel, A.C. Anderson, W.C. Black, J.C. Wheatley, Thermal and magnetic properties of liquid He^3 at low pressure and at very low temperatures, Physics 1 (1965) 337–387 (see Section III.D. 2 as well as Footnote 58 in the references. The pertinent details of these sections are also summarized in [15]).
[15] D.M. Ginsberg, M.J. Melchner, Optimum geometry of saddle shaped coils for generating a uniform magnetic field, Rev. Sci. Instrum. 41 (1970) 122–123.
[16] D.I. Hoult, R.E. Richards, The signal-to-noise ratio of the nuclear magnetic resonance experiment, J. Magn. Reson. 24 (1976) 71–85.

[17] D.I. Hoult, The NMR receiver: a description and analysis of design, Prog. NMR Spectrosc. 12 (1978) 41–77.
[18] F. Roméo, D.I. Hoult, Magnet field profiling: analysis and correcting coil design, Magn. Reson. Med. 1 (1984) 44–65.
[19] H. Hanssum, Exact solution of the Poisson equation for a dc current on a saddle-shaped Helmholtz coil, J. Phys. A 16 (1983) 3385–3392.
[20] H. Hanssum, The magnetic field of saddle-shaped coils: I. Symmetry of the magnetic field around the coil centre, J. Phys. D 17 (1984) 1–18.
[21] H. Hanssum, The magnetic field of saddle-shaped coils: II. Transverse components, J. Phys. D 18 (1985) 1971–1978.
[22] H. Hanssum, The magnetic field of saddle-shaped coils: III. Improving the uniformity of $|\boldsymbol{B}|$ in a large volume, J. Phys. D 19 (1986) 493–501.
[23] J.D. Jackson, Classical Electrodynamics, third ed., Wiley, New York, 1999.
[24] M.A. Brideson, L.K. Forbes, S. Crozier, Determining complicated winding patterns for shim coils using stream functions and the target-field method, Concepts Magn. Reson. 14 (2002) 9–18.
[25] D.J. Griffiths, Introduction to Electrodynamics, second ed., Prentice-Hall, Englewood Cliffs, 1989.
[26] C.P. Bidinosti, I.S. Kravchuk, J. Cha, N.A. David, M.E. Hayden, Wire-wound B_1 coils for low frequency MRI, Proc. Intl. Soc. Mag. Reson. Med. 11 (2004) 1551 (the coil was wound of a contiguous wire $\sim$30 m long and $\sim$1/100 of the wavelength of light at the measurement frequency of 100 kHz. Its self-resonance frequency was 1.9 MHz).
[27] M. Abramowitz, I.A. Stegun, Handbook of Mathematical functions, ninth ed., Dover, New York, 1970 (from identities 9.6.30 and 9.6.31 on pp. 376, $I_m(-\zeta) = (-1)^m I_m(\zeta)$ and $K_m(-\zeta) = (-1)^m K_m(\zeta) - i\pi I_m(\zeta)$ for real $\zeta > 0$).
[28] I.S. Gradshteyn, I.M. Ryzhik, Table of Integrals, Series, Products, fifth ed., Academic Press, Boston, 1994 (see identity 1.353 on pp. 38.).